Zinc ferrite nanoparticles capped with Gongronema latifolium for moderate hyperthermia applications

Article *in* Applied Physics A · February 2022

DOI: 10.1007/s00339-021-05244-8

CITATION
1

READS
123

7 authors, including:

Samson Olatubosun Aisida
University of Nigeria
62 PUBLICATIONS **822** CITATIONS
SEE PROFILE

Ada Agbogu
University of Nigeria
18 PUBLICATIONS **108** CITATIONS
SEE PROFILE

Ishaq Ahmad
National Centre for Physics
152 PUBLICATIONS **1,808** CITATIONS
SEE PROFILE

Applied Physics A (2022) 128:95
https://doi.org/10.1007/s00339-021-05244-8

Applied Physics A
Materials Science & Processing

Zinc ferrite nanoparticles capped with *Gongronema latifolium* for moderate hyperthermia applications

Onah A. Onyedikachi[1] · Samson O. Aisida[1,2,3,4,5] · Ada Agbogu[1] · Ijeh Rufus[6] · Ishaq Ahmad[2,5] · M. Maaza[3,4] · Fabian I. Ezema[1,3,4,7]

Received: 30 September 2021 / Accepted: 28 December 2021

Abstract

Zinc Ferrite Nanoparticles were synthesized using the eco-friendly green synthesis protocol. *Gongronema Latifolium (GL)* leaf extract as a potential reducing and capping agent to influence the properties of ZFNPs for effective hyperthermia application is emplaced in this work. Characterizations techniques such as X-rays diffractometer (XRD), scanning electron microscope (SEM), Fourier transforms infrared (FTIR) spectroscopy, UV–visible spectroscopy and vibrating sample magnetometer were used to determine the properties of the samples. The SEM showed spherical morphology of the samples, XRD spectra revealed the crystallinity with a maximum crystallite size of 30.6 nm, the absorbance surface plasmon resonance peak from the UV result falls within the visible range. The FTIR result showed the various functional group responsible for the reduction of the sample. The VSM confirmed the superparamagnetic nature of the sample. The saturation magnetization increases as the concentration of GL increases. The hyperthermia application properties investigated revealed good specific loss power, which decreases from 207.8 to 105.3 W/g as the concentration of GL increases. Notably, the synthesized nanoparticles have the potential for hyperthermia application in cancer therapy.

Keywords Zinc ferrite · Hyperthermia · Superparamagnetic · *Gongronema Latifolium* · Biomaterials

1 Introduction

Magnetic ferrites have found applications in varying fields, including biomedicine, geology, industries and material physics [1–8]. Magnetic spinel ferrites (MSF) with the basic formula, AB_2O_4, where A are cations of the valency of 1,2,3 or 4–(such as Mn, Zn, Ni, Mg and Co) and B the Fe ion, and they occupy the octahedral and tetrahedral sites, respectively [9–13]. The unusualness of magnetic ferrite is in the magnetic properties that result from the migration of cations between the A and B sites when the temperatures are increased, whereas, at temperatures below the Neel temperature of ~ 10 K, it exhibits antiferromagnetism [14–18]. Among the numerous MSF, zinc ferrite ($ZnFe_2O_4$) nanoparticles have been researched extensively due to their potency in various fields such as in industries, agriculture and biomedicine such as magnetic resonance imaging (MRI) contrast improvement, tissue repair, antimicrobial, anticancer, magnetic hyperthermia and targeted drug delivery [19].

Among these applications, hyperthermia has emerged as a promising treatment method for cancer therapy. In hyperthermia applications, tumorous cells are led to apoptosis and

✉ Samson O. Aisida
samson.aisida@unn.edu.ng

1 Department of Physics and Astronomy, University of Nigeria, Nsukka, Nigeria

2 National Centre for Physics, Quaid-I-Azam University Campus, Islamabad 44000, Pakistan

3 Nanosciences African Network (NANOAFNET), iThemba LABS-National Research, Somerset-West, South Africa

4 UNESCO-UNISA Africa Chair in Nanosciences/Nanotechnology, College of Graduate Studies, University of South Africa (UNISA), Muckleneuk Ridge, P.O. Box 392, Pretoria, South Africa

5 NPU-NCP Joint International Research Center on Advanced Nanomaterials and Defects Engineering, Northwestern Polytechnical University, Xi′an 710072, China

6 Department of Physics, University of Delta, Agbor, Nigeria

7 Africa Centre of Excellence for Sustainable Power and Energy Development (ACE-SPED), University of Nigeria, Nsukka, Nigeria

Published online: 07 January 2022

necrosis due to the temperature rise of the NPs in the range of 41 to 47 °C, owing to lower ability to resist heat than normal healthy cells [20, 21]. For magnetic hyperthermia, an external Radiofrequency (RF) magnetic field is introduced to increase the energy states of the nanoparticles (NPs), which is then transferred to the tumor tissue [22]. Over the years, scientists have used varying experimental techniques and compared different nanoparticles using different thermal thresholds and capping agents to work on hyperthermia.

Research carried out by numerous researchers has shown that the synthesis methods of ferrite nanoparticles play a considerable role in the properties, such as structural, chemical stability, optical & magnetic properties. These methods have been classified as the Bottom-up approach, also known as the building up approach. It involves using substances less complex than the nanoparticles to get the NPs, and the Top-down approach, where nanoparticles are obtained from the disintegration of large molecules [23, 24]. Among the bottom-up methods such as ultrasound irradiation [25], sonochemical approach [26], hydrothermal approach [27], solvothermal method [28], microwave-assisted [29, 30], sol gel [31], Microemulsion [32], Electrochemical method [33, 34], co-precipitation process [35], citrate gel process [36] and biological method [37, 38]. The biological synthesis method, which involves the use of biological reducing and stabilizing agents such as plant extracts, bacteria, fungi, fruit extracts and natural biopolymer, is preferred because it is safer, simpler, environmentally friendly, inexpensive, non-toxic, biocompatible, and does not require high pressures, energy and temperatures [37–41].

Gongronema latifolium is a tropical rainforest plant that belongs to the family *Asclepiadaceae* with hypoglycaemic, hypolipidaemic, anti-inflammatory and antioxidative effects sequel to their phytochemicals (PTC) [42]. Phytochemical (PTC) analysis performed on GL by Chinedu and Friday in 2015 showed the alkaloids, flavonoids, lignans, terpenes, carotenoids and saponin [43]. PTCs are the chemical components that occur naturally and are found in edible fruits and vegetable plants with discrete bio-activities toward animals biochemistry and metabolism substances. These PTC enhanced the reducing and capping potency of the samples.

Herein ZFNPs were synthesized by a green synthesis method using GL extract as a potential reducing and capping agent to enhance their biocompatibility for the stability of the particles for the first time. Various characterization techniques were used to examine the properties of the materials. It's noteworthy that the GL introduced enhanced the properties of the sample and made it suitable for moderate hyperthermia applications.

2 Materials and experimentation

2.1 Materials

Analytical grades of iron nitrate and zinc nitrate, a Sigma Andrich product procured commercially, were used without further purification. Fresh *Gongronema latifolium (Gl)* leaves were sourced locally and were used as a potential reducing and capping agent. Digital pH meter was used to determine the pH of the sample, and distilled water was used for all the synthesis procedures.

2.2 Preparation and production of GL extract

The GL leaves were separated from their stalk and washed thoroughly with distilled water to get rid of dust particles. They were then dried at room temperature for 5 days and ground into powder in an electric mill (Master Chef Electric Blender with Mill). 30 g of the pulverized leaves were mixed with 300 ml of water differently and boiled for 40 min. The extract was then sieved and filtrated with Whatman filter paper. The aqueous extract obtained was stored in a refrigerator at 4 °C.

2.3 Green synthesis of zinc ferrite nanoparticles

8.08 g of iron nitrate and 1.49 g of zinc nitrate–our precursors–were dissolved in 100 and 50 ml of distilled water, respectively, and stirred for 1 h each. These solutions were mixed and stirred on a magnetic stirrer for another 1 h to mix appropriately, and an orange-colored solution was obtained, which had a pH of 4.7. Repeating this procedure two more times gave us three similar solutions in three beakers. 20 ml and 30 ml of GL extract were added gently to the last two solutions, respectively, to form GL-ZFNPs nanoparticles. All three solutions were then dried for 4 h in an oven at a temperature of 60 °C to obtain dried, orange-colored nanoparticles for the uncapped zinc ferrite solution and light brown nanoparticles from the zinc ferrite solution capped with 20 ml and 30 ml extract. The three nanoparticles obtained were then annealed at a temperature of 500 °C for 1 h after which they were packaged for characterization with a label of ZFNPs, GL_{20}_ZFNPs and GL_{30}_ZFNPs.

2.4 Characterization techniques

Powder X-ray diffractograms – which give us the structure of the synthesized $ZnFeO_4$ nanoparticle – were obtained in the 2θ range of 20–80° at room temperature. X-ray Diffraction (XRD) spectra were obtained using Shimadzu diffract meter model XRD 6000. Using Vibrating Sample Magnetometer

(VSM) at room temperature with a maximum applied field of 10kOe, magnetic properties such as saturation magnetization, magneton number were measured. To reveal the size and formation of the morphology of the samples, we performed Scanning electron microscopy (SEM) using Nova Nano SEM 450 (FEI company). Fourier Transform Infrared (FTIR) Spectroscopy and UV–Visible Spectra were done on the samples using the Shimadzu diffract meter model XRD 6000 to identify the chemical bonds in the molecules of the samples by producing an infrared absorption spectrum and to measure the attenuation of a beam of light after it passed through the samples, respectively.

2.5 Hyperthermia application studies

To determine the heating ability of our synthesized nanoparticles, we employed the COMDEL CL-5000, USA RF generator, which uses an alternating magnetic field (AMF) of amplitude 145 Oe at the frequency of 425 kHz and the room temperature of 20 °C using Eq. 1. The results from this setup gave us the temperature–time plots, which translates to the potency of our synthesized nanoparticles for hyperthermia application.

$$\mathrm{SLP} = C\frac{\Delta T}{\Delta t}\frac{V}{m_{\mathrm{ferrite}}} \tag{1}$$

where C is the sample-specific heat capacity, 4185 J/Kg °C, $\frac{\Delta T}{\Delta t}$ is the slope of temperature–time plot measured very close to the origin, V is the sample volume dispersed in 1 ml of distilled water, and m_{ferrite} is the mass of the ferrites in the nanoparticle.

3 Results and discussion

3.1 Structural study of ZFNPs and GL-ZFNPs

The powder X-ray diffraction (XRD) was employed to study the structural properties of the sample. The spectral images as shown in Fig. 1 revealed prominent peaks observed at 2θ with values 28.1˚, 40.3˚, 49.9˚, 58.5˚, 62.5˚ assigned to the plane (220), (311), (400), (422), (5110) and (440). The synthesized ZFNPs were observed to possess a crystalline structure with JCPD No. 82–1049 [44]. Using Scherer's formula given by Eq. 2, the crystallites sizes were obtained as 24.7, 24.1 and 30.6 nm for samples (a), (b) and (c), respectively, as presented in Table 1.

$$D = \frac{k\lambda}{\beta\cos\theta} \tag{2}$$

where D is the average crystallite particle size, K is the shape factor equal to 0.9, λ is the X-ray wavelength, β is the Full Width at Half Maximum (FWHM), and θ is the Bragg angle [45].

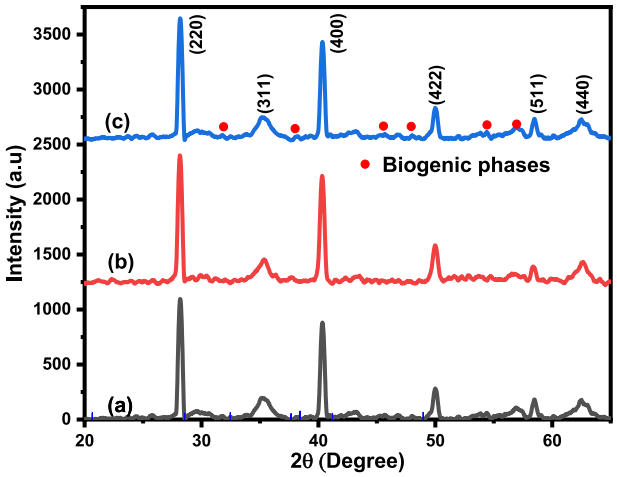

Fig. 1 XRD pattern of **a** ZFNPs **b** GL_{20}- ZFNPs **c** GL_{30}- ZFNPs

The micro-strain (ϖ) of the formulated sample was determined using Eq. 3 from the XRD plane of (400) broadening. The evaluated micro-strain was in line with the crystallite size. This variation observed in the micro-strain shows strain-induced structural changes in the formulated sample.

$$\varpi = \frac{\beta\mathrm{Cos}\theta}{4} \tag{3}$$

The samples' lattice spacing (d) was determined using the Bragg equation (Eq. 4). Also, the lattice parameters were determined using Eq. 5. The lattice space and the parameter were observed to increase from sample a to sample b and later decreased in sample c. the observed variation agrees with the crystallite size. A similar trend was also observed by Aisida et al. [8] with PEG_Ni_ZnONPs [46].

$$\boldsymbol{d} = \frac{\lambda}{2\mathbf{sin}\boldsymbol{\theta}} \tag{4}$$

$$\frac{1}{\boldsymbol{d}^2} = \frac{4}{3}\left(\frac{\boldsymbol{h}^2 + \mathbf{hk} + \boldsymbol{k}^2}{\boldsymbol{a}^2}\right) + \left(\frac{\boldsymbol{l}^2}{\boldsymbol{c}^2}\right) \tag{5}$$

3.2 Morphological study of ZFNPs and GL-ZFNPs

To analyze the morphology of the synthesized samples, a scanning electron microscope (SEM) was employed. Figure 2 shows the SEM images of the samples (a), (b) and c. It can be seen that the sample showed spherical morphology. The degree of resolution increases as the capping agent increases, and the particle is well defined, as seen in the ring of Fig. 2c. As shown in the inset of Fig. 2a–c, the grain size was determined using imageJ

Table 1 Crystallite size, particle size and the magnetic properties of the samples

Samples	*D*(nm)	*Xc*	E_g (eV)	d(nm)	a (nm)	Π
ZFNPs	24.7	17.4 ± 16	2.23	0.2232	1.0309	0.10049
GL_{20}_ZFNPs	24.1	19.3 ± 17	2.31	0.2237	1.0332	0.10720
GL_{30}_ZFNPs	30.6	21.8 ± 10	2.65	0.2232	1.0332	0.10049

D Crystallite size; M_s Saturation magnetization, M_r Remanence, H_c Coercivity, E_g Energy bandgap and *Xc* = Grain size

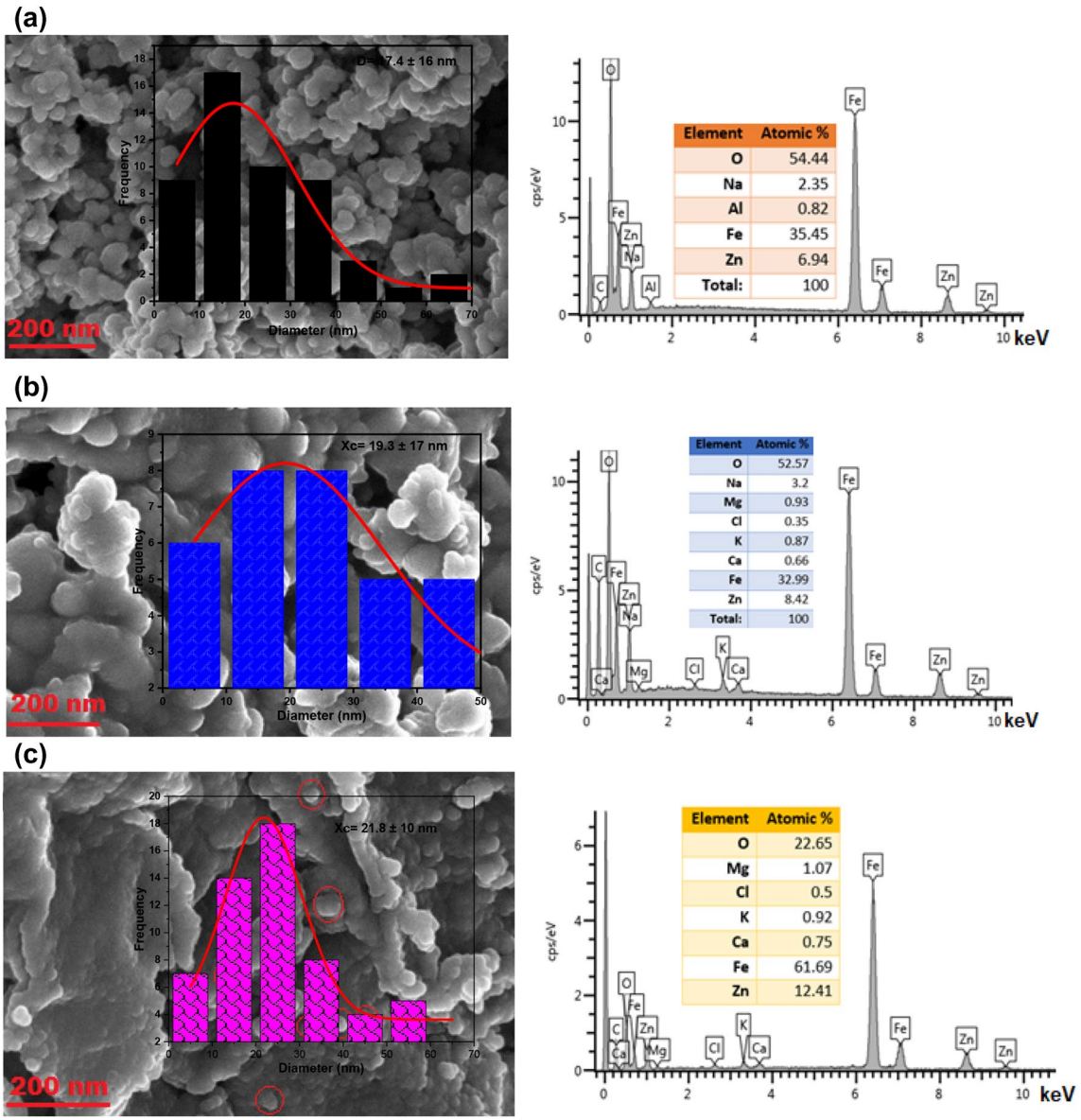

Fig. 2 SEM and EDX images of **a** ZFNPs **b** GL_{20}- ZFNPs **c** GL_{30}- ZFNPs

software, and the estimated grain size is between 17 and 21 nm. The grain size was observed to increase gradually as the dopant concentration increased. All the elements in the compound and the extract are presented by the energy dispersive X-rays diffraction (EDXD), as seen in the right section of Fig. 2. Peaks of Fe, Zn, O and C showed on the EDX spectra confirmed their presence in the samples, with Fe having the most prominent peak followed by Zn. The elements Mg, K and Ca are introduced from the content of the extract.

3.3 Optical properties of ZFNPs and GL-ZFNPs

UV–visible spectroscopy technique was employed to determine the optical properties of the synthesized nanoparticles. Figure 3i shows the absorption spectra of the prepared samples. The notable peaks at 375, 374 and 373 nm for sample a, b and c, respectively, were observed to fall within the visible range 350–450 nm and therefore confirms the formation of ZFNPs as noted by Almessiere [47]. Figure 3ii shows the direct estimated energy bandgap (E_g) of the samples using the Kubelka–Munk (KM) and Tauc plot equations as presented in Eqs. 6 and 7.

$$F(R) = \frac{\alpha}{s} = \frac{(1-R)^2}{2R} \tag{6}$$

$$(\alpha h\nu)^2 = A(h\nu - E_g) \tag{7}$$

where F(R) represents the Kubelka–Munk function; α = absorption, and R represent the reflectance. We observed an increase in E_g to the increase in the dopant concentration. The observed increase was relative to the grain size, as presented in Table 1. Studies have confirmed that various factors such as dopant concentrations, annealing, particle size and some impurities can influence the values of E_g [48–50].

3.4 FTIR properties of ZFNPs and GL-ZFNPs

The FTIR spectra show the functional group in GL responsible for the reduction and functionalization of the sample in the absorption bands between 4000–500 cm^{-1}, as shown in Fig. 4. There appears to be a shift in the peak's wavelength due to doping; hence our dopant serves as a potential reducing agent. The peak of the samples in the range of 3300–3500 cm^{-1} corresponds to the hydroxyl (–OH) stretching of water molecules. The peak around 1030 cm^{-1} corresponds to amine (C–N) Stretching. A characteristic peak at about 570 cm^{-1} is attributed to the formation of FeO [38, 51].

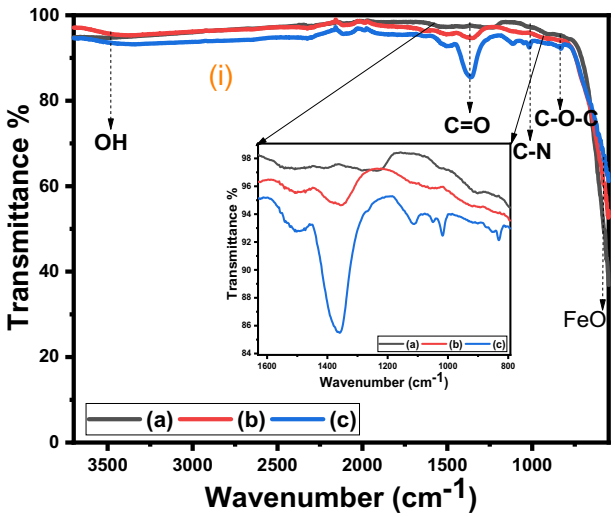

Fig. 4 FTIR spectra of **a** ZFNPs **b** GL_{20}- ZFNPs (c) GL_{30}- ZFNPs

3.5 Magnetic properties of ZFNPs and GL-ZFNPs

The magnetic properties of the samples were analyzed using a vibrating sample magnetometer (VSM). The plot of the magnetic field against magnetization is presented in Fig. 5. The hysteresis loop shape shows that the samples moved from ferromagnetic to superparamagnetic characteristics as the concentration of the dopant increased. This agrees with state-of-the-art results showing the effect of the dopant on the magnetic properties [11, 52, 53]. Magnetic parameters of the samples such as saturation magnetization (M_s), remanence magnetization (M_r) and coercivity (H_i) were obtained as presented in Table 2. The samples' remanence

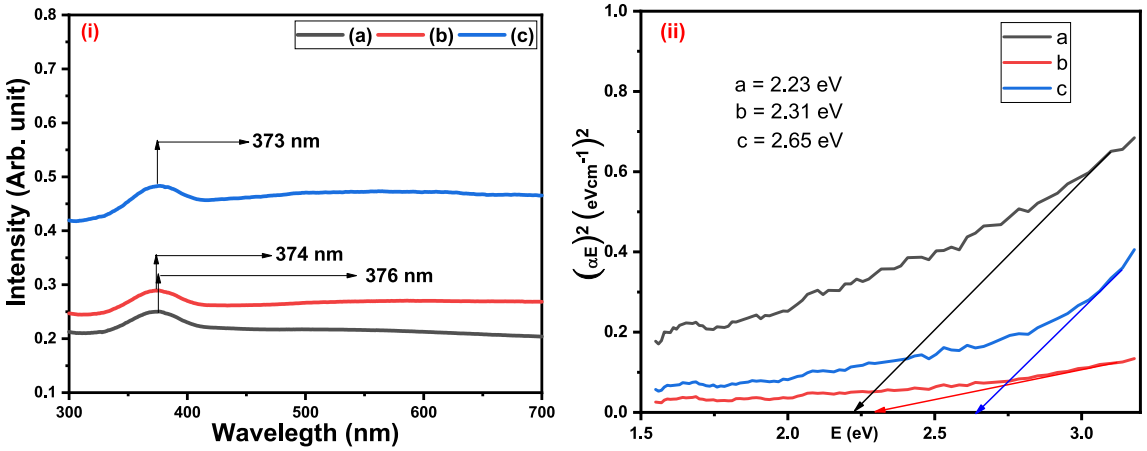

Fig. 3 (i) UV–visible spectra (ii) Energy bandgap of **a** ZFNPs **b** GL_{20}- ZFNPs **c** GL_{30}- ZFNPs samples

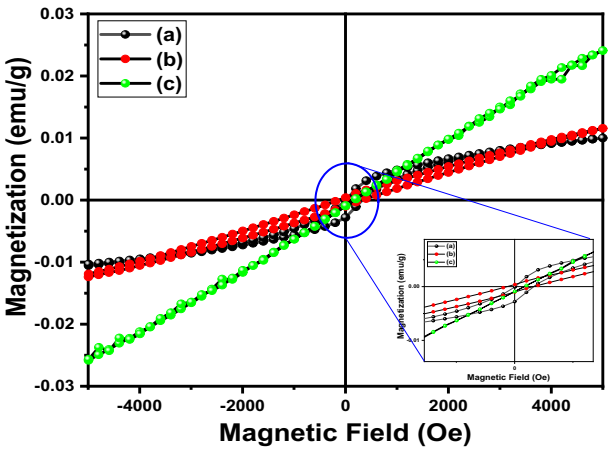

Fig. 5 The VSM analysis of **a** ZFNPs **b** GL_{20}- ZFNPs **c** GL_{30}- ZFNPs

magnetization was approximately zero for sample c, showing superparamagnetic behavior. The saturation magnetization was observed to increase with the capping agent. The observed increase in the saturation magnetization agrees with Aisida et al., 2019 considering the effect of PVA, PVP and PEG on the magnetic properties of Zinc ferrite [54]. The magnetic properties can also be influenced by the crystallite size of the sample and the doping agent [37, 55]. The formulated sample showed lower Ms than the bulk values of 93.9 emu/g described by Kombaiah et al. [56]. The observed increase in the saturation magnetization that we adduced to the cation inversion distribution among the A-B interstitial sites [57, 58].

3.6 Hyperthermia heating measurement

The temperature–time curves of the three (3) samples in the presence of an applied magnetic field of strength 145 Oe at the room temperature of 20 °C are presented in Fig. 6. From the figure, the heating ability of the samples as well as their Specific Loss Power (SLP) were deduced as shown in Table 2. It can be clearly seen that the concentration of the encapsulating material affected the heating ability of the nanoparticle immensely. The heating temperature of the uncapped ZF particle reduced from 46.99 to 40.81 °C when capped with the highest concentration of the extract. The best suitable therapeutic temperature range for the necrosis of tumorous cells is 40–48 °C [37]**;** thus, GL_{20}-ZFNP is best suited for hyperthermia application. Aisida et al. [8], in their work, observed that polymers such as Polyethylene glycol (PEG) help to reduce the heating temperature to the therapeutic temperature range [8].

The SLP, a determinant of the induction heating ability of the magnetic nanoparticle, was calculated using Eq. 1. The SLP value of the ZFNPs calculated to be 207.8 W/g,

Table 2 Heating ability and SLP values of our samples

Samples	M_s (emu/g)	M_r (emu/g)	M_r/M_s	H_c (Oe)	$\Delta T/\Delta t$ (C/s)	SLP (W/g)	ΔT (℃)	T
ZFNPs	0.0101	0.00028	0.0277	193.79	0.4569	207.8	26.99	46.99
GL_{20}_ZFNPs	0.0115	0.0042	0.0365	184.67	0.3134	142.6	25.05	45.05
GL_{30}_ZFNPs	0.0242	0.001	0.0413	155.04	0.2315	105.3	20.81	40.81

Total temperature (T) = room temp. (20 ℃) + ΔT (℃)

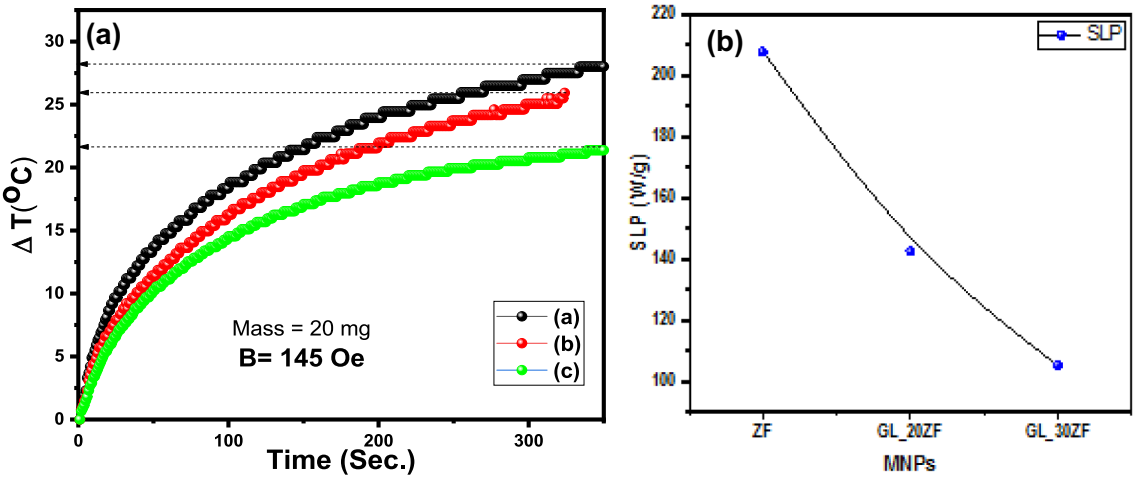

Fig. 6 **a** The temperature–time plot obtained after the application of 145 Oe magnetic field and **b** The quantitative comparison of the SLP (W/g) for ZF, GL_{20}-ZF and GL_{30}-ZF

was higher than that for the samples capped with GL. The estimated SLP for GL_{20}-ZF and GL_{30}-ZF was 142.6 W/g and 105.3 W/g, respectively. Hence, the SLP is observed to decrease significantly with the capping agent. Jadhav, et al. [59], who synthesized gadolinium-substituted manganese zinc ferrite nanoparticles G-MZF, observed decreasing values of SLP with an increase in the gadolinium content [59]. SLP results differ from author to author depending on their techniques for estimating SLP and other characteristics such as the frequency, magnetic field strength and ferrite materials' concentration [37].

4 Conclusion

Zinc Ferrite Nanoparticles (ZFNPs) were synthesized using the eco-friendly green synthesis protocol. In this work, *Gongronema Latifolium* extract was used as a potential reducing and capping agent with potential influence on the effectiveness of hyperthermia ability on the sample. Characterizations such as XRD, SEM, EDX and VSM showed that the produced NPs possessed properties that made them suitable for hyperthermia application. The SEM showed spherical morphology of the samples, XRD spectra analysis revealed the maximum crystallite size of 30.6 nm for GL_{30}-ZF. The VSM confirmed the superparamagnetic nature of GL_{30}-ZF. The introduction and the subsequent increase of the concentration of GL extract led to the reduction of the heating temperature within the therapeutic range, with GL_{20}-ZF showing the best heating ability. Further investigations for the hyperthermia application were carried out on the formulated samples by estimating their specific loss power (SLP). The SLP values were observed to decrease from 207.8 to 105.3 W/g. Notably, the synthesized nanoparticles have the potential for hyperthermia application in cancer therapy.

Acknowledgements SOA and FIE acknowledged TETFUND under the contract number (TETFUND/DR&D/CE/UNI/NSKKA/RP/VOL.1). SOA acknowledges the NCP-TWAS Postdoc Fellowship award for the success of this work (NCP-CAAD/TWAS_Fellow8408).

FIE acknowledges the support received from the Africa Centre of Excellence for sustainable Power and Energy Development (ACE-SPED), University of Nigeria, Nsukka

References

1. R.H. Kodama, Magnetic nanoparticles. J. Magn. Magn. Mater. **200**, 359–372 (1999)
2. D. Vollath, Book review - nanomaterials an introduction to synthesis, properties and application. Environ. Eng. Manage. **7**(6), 865–870 (2008)
3. V. Skumryev, S. Stoyanov, Y. Zhang, G. Hadjipanayis, D. Givord, J. Nogués, Beating the superparamagnetic limit with exchange bias. Nature Res. J. **423**, 850–853 (2003)
4. S. Laurent, D. Forge, M. Port, A. Roch, C. Robic, L. Vander Elst, R.N. Muller, Magnetic iron oxide nanoparticles: synthesis, stabilization, vectorization, physicochemical characterizations, and biological applications. Chem. Rev. **110**, 2574–2574 (2010)
5. J. Zhang, M. Saltzman, Engineering biodegradable nanoparticles for drug and gene delivery. Chem. Eng. Prog. **109**, 25–30 (2013)
6. N.C. Mueller, B. Nowack, Exposure modeling of engineered nanoparticles in the environment. Environ. Sci. Technol. **42**(12), 4447–4453 (2008)
7. E.A. Rogozea, A.R. Petcu, N.L. Olteanu, C.A. Lazar, D. Cadar, M. Mihaly, Tandem adsorption-photodegradation activity induced by light on NiO-ZnO p–n couple modified silica nanomaterials. Mater. Sci. Semicond. Process. **57**, 1–11 (2017)
8. S.O. Aisida, M.H.B.S. Alnasir, A.K.H. Bashir, R. Bucher, I. Ahmad, T. Zhao, M. Maaza, F.I. Ezema, The role of polyethylene glycol on the microstuctural, magnetic and specific absorption rate in thermoablation of Mn-Zn ferrite nanoparticles by sol-gel protocol. Eur. Polym. J. **132**, 109739 (2020)
9. R. Valenzuela, Novel applications of ferrites. Phys. Res. Int. **2012**, 1–9 (2012)
10. T. Dippong, E.A. Levei, O. Cadar, Formation, structure and magnetic properties of MFe2O4@SiO2(M = Co, Mn, Zn, Ni, Cu) nanocomposites. Materials **14**, 1139 (2021)
11. T. Dippong, O. Cadar, E.A. Levei, I.G. Deac, L. Diamandescu, L. Barbu-Tudoran, Influence of cobalt ferrite content on the structure and magnetic properties of (CoFe2O4)X (SiO2-PVA)100-X nanocomposites. Ceram. Int. **44**(7), 7891–7901 (2018)
12. T. Dippong, E.A. Levei, C. Tanaselia, M. Gabor, M. Nasui, L.B. Tudoran, G. Borodi, Magnetic properties evolution of the CoxFe3-xO4/SiO2 system due to advanced thermal treatment at 700 °C and 1000 °C. J. Magn. Magn. Mater. **410**, 47–54 (2016)
13. A.M. Almessiere, Y. Slimani, S. Guner, M. Sertkol, A.K. Demir, S.E. Shirsath, A. Baykal, Sonochemical synthesis and physical properties of Co0.3Ni0.5Mn0.2EuxFe2−xO4 nano-spinel ferrites. Ultrason. Sonochem. **58**, 104654 (2019)
14. S. Ayyappan, G. Paneerselvam, M.P. Antony, J. Philip, Structural stability of ZnFe2O4 nanoparticles under different annealing conditions. Mater. Chem. Phys. **128**, 400–404 (2011)
15. A.D. Korkmaz, S. Güner, Y. Slimani, H. Gungunes, M. Amir, A. Manikandan, A. Baykal, Microstructural, optical, and magnetic properties of vanadium-substituted nickel spinel nanoferrites. J. Supercond. Nov. Magn. **32**, 1057–1065 (2019)
16. M. Almessiere, Y. Slimani, M. Sertkol, F. Khan, M. Nawaz, H. Tombuloglu, E.A. Al-Suhaimi, A. Baykal, Ce–Nd Co-substituted nanospinel cobalt ferrites: an investigation of their structural, magnetic, optical, and apoptotic properties. Ceram. Int. **45**(13), 16147–16156 (2019)
17. M. Almessiere, Y. Slimani, H. Güngüneş, H.E. Sayed, A. Baykal, AC susceptibility and Mossbauer study of Ce3+ ion substituted SrFe12O19 nanohexaferrites. Ceram. Int. **44**, 10470–10477 (2018)
18. Y. Slimani, M. Almessiere, S.E. Shirsath, E.H. Ghulam, A. Yasin, B.O. Baykal, I. Ercan, Investigation of structural, morphological, optical, magnetic and dielectric properties of (1-x)BaTiO3/xSr0.92Ca0.04Mg0.04Fe12O19 composites. J. Magn. Magn. Mater. **510**, 166933 (2020)
19. S. Akhtar, S. Rehman, M.A. Almessiere, F.A. Khan, Y. Slimani, A. Baykal, Synthesis of Mn0.5Zn0.5SmxEuxFe1.8−2xO4 nanoparticles via the hydrothermal approach induced anti-cancer and anti-bacterial activities. Nanomaterials **9**, 1635 (2019)
20. P. Cherukuri, E.S. Glazer, S.A. Curley, Targeted hyperthermia using metal nanoparticle. Adv. Drug Deliv. Rev. **62**, 339–345 (2010)
21. I. Sharifi, H. Shokrollahi, S. Amiri, Ferrite-based magnetic nanofluids used in hyperthermia. J. Magn. Magn. Mater. **324**, 903–915 (2012)

22. R. Sharma, C.J. Chen, Newer nanoparticles in hyperthermia treatment and thermometry. J. Nanopart. Res. **11**, 671–689 (2009)
23. S. Iravani, Green synthesis of metal nanoparticles using plants. Green Chem. **13**, 2638 (2011)
24. T. Dippong, E.A. Levei, O. Cadar, Recent advances in synthesis and applications of MFe2O4 (M = Co, Cu, Mn, Ni, Zn) nanoparticles. Nanomaterials **11**, 1560 (2021)
25. Y. Slimani, M.A. Almessiere, M. Sertkol, S.E. Shirsath, A. Baykal, M. Nawaz, S. Akhtar, B. Ozcelik, I. Ercan, Structural, magnetic, optical properties and cation distribution of nanosized Ni0.3Cu0.3Zn0.4TmxFe2−xO4 ($0.0 \leq x \leq 0.10$) spinel ferrites synthesized by ultrasound irradiation. Ultrason. Sonochem. **57**, 203–211 (2019)
26. Y. Slimani, B. Unal, M. Almessiere, A.D. Korkmaz, S.E. Shirsath, G. Yasin, A. Trukhanov, A. Baykal, Investigation of structural and physical properties of Eu3+ ions substituted Ni0.4Cu0.2Zn0.4Fe2O4 spinel ferrite nanoparticles prepared via sonochemical approach. Results Phys. **17**, 103061 (2020)
27. M.A. Almessiere, Y. Slimani, M. Sertkol, M. Nawaz, A. Sadaqat, A. Baykal, I. Ercan, B. Ozçelik, Effect of Nb3+ substitution on the structural, magnetic, and optical properties of Co0.5Ni0.5Fe2O4 nanoparticles. Nanomaterials **9**, 430 (2019)
28. B. Mahltig, E. Gutmann, M. Reibold, D. Meyer, H. Bottcher, Synthesis of Ag and Ag/SiO2 sols by solvothermal method and their bactericidal activity. J Sol-Gel Sci Technol. **51**, 204–214 (2009)
29. J. Chen, K. Wang, J. Xin, Y. Jin, Microwave-assisted green synthesis of silver nanoparticles by carboxymethyl cellulose sodium and silver nitrate. Mater. Chem. Phys. **108**, 421–424 (2008)
30. F.N. Sayed, V. Polshettiwar, Facile and sustainable synthesis of shaped iron oxide nanoparticles: effect of iron precursor salts on the shapes of iron oxides. Sci. Rep. **5**, 9733 (2015)
31. Y. Slimani, M.A. Almessiere, S. Güner, N.A. Tashkandi, A. Baykal, M.F. Sarac, M. Nawaz, I. Ercan, Calcination effect on the magneto-optical properties of vanadium substituted NiFe2O4 nanoferrites. J. Mater. Sci.: Mater. Electron. **30**(10), 9143–9154 (2019)
32. P. Cozzoli, R. Comparelli, E. Fanizza, M. Curri, A. Agostiano, D. Laub, Photocatalytic synthesis of silver nanoparticles stabilized by TiO2 nanorods: a semiconductor/metal nanocomposite in homogeneous nonpolar solution. J. Am. Chem. Soc. **126**, 3868–3879 (2004)
33. H. Ma, B. Yin, S. Wang, Y. Jiao, W. Pan, S. Huang, S. Chen, F. Meng, Synthesis of silver and gold nanoparticles by a novel electrochemical method. Chem. Phys. Chem. **24**, 68–75 (2004)
34. Y. Zhang, F. Chen, J. Zhuang, Y. Tang, D. Wang, Y. Wang, A. Donga, N. Ren, Synthesis of silver nanoparticles via electrochemical reduction on compact zeolite film modified electrodes. Chem. Commun. **24**, 2814–2815 (2002)
35. S. Laurent, D. Forge, M. Port, A. Roch, C. Robic, E.L. Vander, R. Muller, Magnetic iron oxide nanoparticles: synthesis, stabilization, vectorization, physicochemical characterizations, and biological applications. Chem. Rev. **108**, 2064–2121 (2008)
36. M. Almessiere, Y. Slimani, A. Trukhanov, A. Baykal, H. Gungunes, E. Trukhanova, S.V. Trukhanov, V. Kostishin, Strong correlation between Dy3+ concentration, structure, magnetic and microwave properties of the [Ni0.5Co0.5](DyxFe2-x)O4 nanosized ferrites. J. Ind. Eng. Chem. **90**, 251–259 (2020)
37. S.O. Aisida, A. Ali, O.E. Oyewande, I. Ahmad, A. Ul-Hamid, T.-K. Zhao, M. Maaza, F.I. Ezema, Biogenic synthesis enhanced structural, morphological, magnetic and optical properties of zinc ferrite nanoparticles for moderate hyperthermia applications. J. Nanopart. Res. **23**, 47 (2021)
38. S.O. Aisida, N. Madubuonu, M.H. Alnasir, I. Ahmad, S. Botha, M. Maaza, F.I. Ezema, Biogenic synthesis of iron oxide nanorods using Moringa oleifera leaf extract for antibacterial applications. Appl. Nanosci. **10**, 305–315 (2020)
39. T. Dippong, E.A. Levei, F. Goga, I. Petean, A. Avram, O. Cadar, The impact of polyol structure on the formation of Zn0.6Co0.4Fe2O4 spinel-based pigments. J. Sol-Gel Sci. Technol. **192**, 736–744 (2019)
40. M.A. Almessiere, Y. Slimani, S. Rehman, F.A. Khan, M. Sertkol, A. Baykal, Green synthesis of Nd substituted Co-Ni nanospinel ferrites: a structural, magnetic, and antibacterial/anticancer investigation. J. Phys. D: Appl. Phys. **55**, 055002 (2021)
41. M.A. Almessiere, Y. Slimani, I.A. Auwal, S.E. Shirsath, M.A. Gondal, M. Sertkol, A. Baykal, Biosynthesis effect of Moringa oleifera leaf extract on structural and magnetic properties of Zn doped Ca-Mg nano-spinel ferrites. Arab. J. Chem. **14**(8), 103261 (2021)
42. N. Ugochukwu, N. Babady, Anti hyperglycemic effect of aqueous and ethanol extracts of Gongronema latifolium leaves on glucose and glycogen metabolism in livers of normal and Streptozotocin. J. Life Sci. **73**(15), 1925–1938 (2003)
43. I. Chinedu, O.U. Friday, Phytochemical analysis of gongronema latifolium benth leaf using gas chromatographic flame ionization detector. Int. J. Chem. Biomol. Sci. **1**(2), 60–68 (2015)
44. P. Thandapani, M.R. Viswanathan, J.C. Denardin, Magnetocaloric effect and universal curve behavior in superparamagnetic zinc ferrite nanoparticles synthesized via microwave assisted co-precipitation method. Phys. Status Solidi **215**(11), 1700842 (2018)
45. B. Cullity, *Elements of X-ray diffraction* (Addison-Wesley, London, 1978)
46. S.O. Aisidaa, A. Batool, F.M. Khanf, L. Rahmanf, A. Mahmoodg, I. Ahmadb, T.-K. Zhaoh, M. Maaza, F.I. Ezema, Calcination induced PEG-Ni-ZnO nanorod composite and its biomedical applications. Mater. Chem. Phys. **255**, 123603 (2020)
47. M.A. Almessiere, Y. Slimani, U. Kurtan, S. Guner, M. Sertkol, S.E. Shirsath, S. Akhtar, A. Baykal, I. Ercan, Structural, magnetic, optical properties and cation distribution of nanosized Co0.7Zn0.3TmxFe2−xO4 ($0.0 \leq x \leq 0.04$) spinel ferrites synthesized by ultrasonic irradiation. Ultrason. Sonochem. **58**, 104638 (2019)
48. T.R. Tatarchuk, N.D. Paliychuk, M. Bououdina, B. Al-Najar, M. Pacia, W. Macyk, A. Shyichuk, Effect of cobalt substitution on structural, elastic, magnetic and optical properties of zinc ferrite nanoparticles. J. Alloy. Compd. **731**, 1256–1266 (2018)
49. M. Almessiere, Y. Slimani, S. Guner, M. Nawaz, A. Baykal, F. Aldakheel, A. Sadaqat, I. Ercan, Effect of Nb substitution on magneto-optical properties of Co0.5Mn0.5Fe2O4 nanoparticles. J. Mol. Struct. **1195**, 269–279 (2019)
50. Y. Slimani, M.A. Almessiere, S. Guner, F.S. Alahmari, G. Yasin, A.V. Trukhanov, A. Baykal, "Influence of Tm–Tb substitution on magnetic and optical properties of Ba–Sr hexaferrites prepared by ultrasonic assisted citrate sol-gel approach. Mater. Chem. Phys. **253**, 123324 (2020)
51. A. Ghasemi, M. Reza, S.T. Loghman-Estarki, M. Tavoosi, "The microstructure and magnetic behavior of spark plasma sintered iron/nickel zinc ferrite nanocomposite synthesized by the complex sol-gel method. Compos. Part B: Eng. **175**, 107179 (2019)
52. M. Ognjanovic, D.M. Stankovic, Y. Ming, H. Zhang, B. Jancar, B. Dojcinovic, Z. Prijovic, B. Antic, Bifunctional (Zn, Fe)3O4 nanoparticles: Tuning their efficiency for potential application in reagentless glucose biosensors and magnetic hyperthermia. J. Alloy. Compd. **777**, 454–462 (2019)
53. G.R. Gordani, M.R.L. Estarki, E. Kiani, S. Torkian, The effects of strontium ferrite micro-and nanoparticles on the microstructure, phase, magnetic properties, and electromagnetic waves absorption of graphene oxide-SrFe12O19-SiC aerogel nanocomposite. J. Magn. Magn. Mater. **545**, 168667545 (2022)
54. S.O. Aisida, P.A. Akpa, I. Ahmad, M. Maaza, F.I. Ezema, Influence of PVA, PVP and PEG doping on the optical, structural,

morphological and magnetic properties of zinc ferrite nanoparticles produced by thermal method. Physica B **571**, 130–136 (2019)
55. M. Ahangar, A. Hashim, Synthesis and characterization of manganese ferrite nanoparticles by thermal treatment method. J. Magn. Magn. Mater. **323**, 1745–1749 (2011)
56 K. Kombaiah, J.V.J.K.L. John, M.J. Bououdina, R. Ramalingam, Okra extract-assisted green synthesis of CoFeO nanoparticles and their optical, magnetic and antimicrobial properties. Mater. Chem. Phys. **204**, 410–419 (2018)
57. V. Grant, K. John, P. Peter, R. Sergey, V. Shen, The effect of different Fe concentrations on the structural and magnetic properties of near-surface superparamagnetic Ni1− xFex nanoparticles in SiO2 made by dual low energy. J. Magn. Magn. Mater. **473**, 125–130 (2018)
58. G.R. Gordani, M.R.L. Estarki, M. Danesh, E. Kiani, M. Tavoosi, Microstructure, phase, magnetic properties, and electromagnetic wave absorption of graphene oxide –aerogel. Ceram. Int. **2**, 41 (2021)
59. S.V. Jadhav, P.S. Shewale, B.C. Shin, M.P. Patil, G.D. Kim, A.A. Rokade, S.S. Park, R.A. Bohara, Y.S. Yu, Study of structural and magnetic properties and heat induction of gadolinium-substituted manganese zinc ferrite nanoparticles for in vitro magnetic fluid hyperthermia. J. Colloid Interface Sci. **541**, 192–203 (2019)